electronics

MDPI

Article

Fast Readout of Split-Ring Resonators Made Simple and Low-Cost for Application in HPLC

Moritz Hitzemann *, Kirsten J. Dehning, Adrian V. Gehl, Erk-Fietje Sterr and Stefan Zimmermann

Department of Sensors and Measurement Technology, Institute of Electrical Engineering and Measurement Technology, Leibniz Universität Hannover, Appelstr. 9A, 30167 Hannover, Germany; dehning@geml.uni-hannover.de (K.J.D.); adrian.gehl@ims.uni-hannover.de (A.V.G.); e.f.sterr@web.de (E.-F.S.); zimmermann@geml.uni-hannover.de (S.Z.)

* Correspondence: hitzemann@geml.uni-hannover.de; Tel.: +49-511-762-14649

Abstract: Split-ring resonators (SRR) are simple electrical circuits that show a significant shift in resonance frequency even with the smallest changes in split capacitance, and thus in permittivity, electric conductivity, and dielectric losses of the split capacitor's dielectric. Usually, the resonance frequency is derived from the frequency response, but recording the frequency spectrum takes a certain amount of time. Here, we present a new capillary split-ring resonator CaSRR with fast readout for liquid chromatography (LC), which is capable of accurately detecting very fast changes in split capacity. The proposed method is based on the detection of the transmitted signal at a single frequency that is analyzed by demodulation. The demodulated signal changes its amplitude depending on the shift of the resonance frequency. Our simple low-cost electronics enables an average sampling rate of 42 Hz with 128 averages of the demodulated signal and has a frequency stability of 840 mHz. Thus, a minimum change in permittivity of $\Delta\varepsilon_{r,min} = 11.26 \times 10^{-3}$ can be detected. Finally, a chromatogram of one sugar (glucose) and one sugar alcohol (xylitol) is recorded using the SRR and is compared to a standard refractive index detector.

Keywords: split-ring resonator; SRR; liquid chromatography; LC; readout electronics; demodulator; HPLC

Citation: Hitzemann, M.; Dehning, K.J.; Gehl, A.V.; Sterr, E.-F.; Zimmermann, S. Fast Readout of Split-Ring Resonators Made Simple and Low-Cost for Application in HPLC. *Electronics* **2022**, *11*, 1139. https://doi.org/10.3390/electronics11071139

Academic Editor: Farhad Rachidi

Received: 8 March 2022
Accepted: 2 April 2022
Published: 4 April 2022

1. Introduction

Split-ring resonators (SRR) significantly shift their resonance frequency even with the smallest change in split capacitance, and thus in permittivity, dielectric losses, and conductivity of the split capacitor's dielectric. This effect makes split-ring resonators increasingly attractive for various applications, such as (bio)chemical sensors for the detection of biomarkers in medical applications [1–3] and the dielectric characterization of thin films and liquids [4–6]. Here, the dielectric characterization of liquids inside a capillary is of particular interest [7–9]. The use of liquid chromatography (LC), e.g., high performance/pressure liquid chromatography (HPLC) and ion chromatography (IC), for the physical separation of compounds in a liquid phase is used in a wide variety of applications such as food, drug, and environmental analysis; process monitoring in the chemical industry; and even bioreactors [10–12]. This wide variety of applications pose special challenges for the detectors used, which have to detect multiple types of substances. Depending on the different compound properties, the detection principles can be divided into light-based detectors (such as fluorescence, absorption, refraction, and scattering) and resistive detectors [13]. For some compounds, additional sample preparation is required to be detected by optical detectors [14]. Other detectors, such as mass spectrometers, have high initial and operating costs, but can provide a second dimension of separation [13]. We aim for the development of a new universal detector for liquid chromatography (LC) based on a simple but sensitive SRR that is easy to integrate and is compatible with LC due to its special split-ring structure made from capillaries. This special SRR design will be part of another publication. Here, we focus on new readout electronics.

LC detectors require fast response times of 1 s or less to resolve fast peaks eluting from the LC column [15]. Therefore, this work concentrates on the development of a fast readout method for SRR [16–18].

The most common method for determining the frequency response of SRR and other resonant oscillating measurement systems is a vector network analyzer (VNA), which records the frequency response of SRR with a frequency sweep in the required frequency range in order to display/determine the frequency response of the SRR [19,20]. However, measuring the frequency response of SRR even over a small frequency range, but at a high frequency resolution, as required for accurate determination of the resonance frequency and the frequency shift, can take several seconds or even minutes—too long for resolving the peaks eluting from the LC column. Another common way of evaluating resonant oscillating measurement systems such as quartz microbalances is measuring the exponential decay [21]. This method requires very fast and complex data acquisition that must operate at minimum double the resonant frequency of the sensor in order to capture the exponential decay. Thus, our approach uses a constant measuring frequency, instead of analyzing a certain frequency range or the exponential decay, to determine the resonance frequency shift. Therefore, SRR is excited at a constant frequency that is shifted to the resonance frequency of the SRR. Thus, a changing resonance frequency modulates the amplitude of the transmitted excitation signal. Demodulating this signal results in an output signal that correlates to the resonance frequency shift of the SRR. To the best of our knowledge, this approach of monitoring a resonant oscillating measurement system based on a single transmitted frequency has not been reported yet. This allows for the detection of even the smallest changes in split capacity in real time by just analyzing the transmission signal of the SRR at a defined frequency. Due to the very high sampling rate of the ADC and microcontroller with 5.4 kS/s, the transmission signal can be averaged to increase the signal-to-noise ratio (SNR) and to improve the limits of detection while still resolving the chromatogram.

2. Materials and Methods

Split-ring resonators are simplified LCR resonant circuits built from a ring structure with a split coupled to a microstrip transmission line, as shown in Figure 1. At resonance frequency, most of the supplied energy is magnetically coupled into the split-ring structure and forms a standing wave. Therefore, a strong electric field is localized inside the split. The split is a simple capacitor that changes its capacitance depending on the electromagnetic properties of the surrounding materials. A change in the capacitance leads to a shift in resonance frequency [3,22–24]. For example, a higher permittivity reduces the resonance frequency of the split-ring structure. In most sensor applications, SRRs have relatively large capacitors, leading to significant resonance frequency shifts and the highest sensitivity. In LC, the peak volume is limited to a few µL, requiring a small detector volume for keeping the LC resolving power, and thus, a small split capacitor, but limiting the sensitivity.

Therefore, we use a new low-volume SRR concept that is easy to integrate and is compatible with LC. The new split-ring structure, as shown in Figure 1, is made of a copper capillary with outer diameter (OD) of 1.6 mm and inner diameter (ID) of 0.3 mm, as well as a Vici Valco PEEK union ID of 1.6 mm. The capillary split-ring shown in Figure 1 is approximately 20 mm × 40 mm with an effective length of 121 mm resulting in a total volume of 8.6 µL. The area enclosed by the split-ring is 845 mm^2. The distance between the ends of the capillaries inside the PEEK union—namely the split capacitor—is 1.2 mm and the capacitor has an area of 1.94 mm^2, resulting in a total volume of about 2.3 µL. However, it should be noted that this volume depends on the manufacturing tolerances of the PEEK union and the polished capillary ends. The electromagnetic wave is coupled via a 50 mm long transmission line made of a simple printed circuit board with dielectric material RO4003C of 0.5 mm thickness with 50 mm × 20 mm. The transmission line has a width of 1.12 mm. The split-ring is fixed on top of the transmission line with a 0.15 mm thick isolation layer made of 3M 5413 polyimide adhesive tape in between. This capillary split-ring resonator (CaSRR) is designed specifically as a detector for high performance liquid

chromatography (HPLC) [18] due to its low containment volume and easy integration with LC, without any compatibility issues between the solvents and the CaSRR materials.

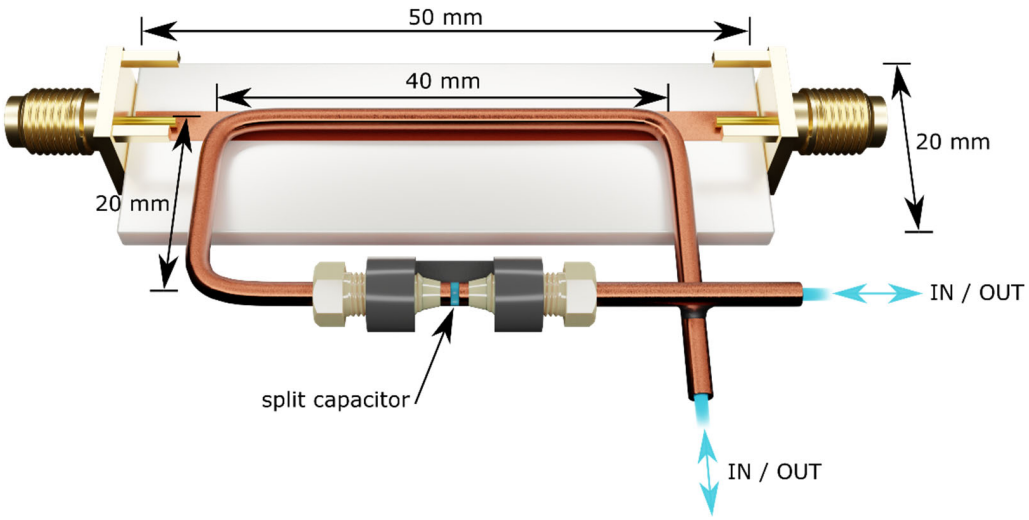

Figure 1. Schematic of the capillary split-ring resonator (CaSRR) with a transmission line on RO4003C PCB and a split-ring made of copper capillaries. The split capacitor is formed inside a Vici Valco PEEK union with an inner diameter of 1.6 mm by the two opposite capillary endings.

The basic principle of the new readout electronics is shown in Figure 2. A waveform generator supplies the transmission line of the CaSRR with a frequency-controlled sine wave. Due to the band rejection filter characteristics of CaSRR, all frequencies can pass the system through the transmission line, except for frequencies near the resonance frequency of CaSRR. The stop bandwidth of the band rejection filter is mainly defined by the quality factor of CaSRR. Finally, the output signal from CaSRR is demodulated via a diode and a capacitor, as shown in Figure 2. The used envelope demodulator detects the envelope of the transmitted CaSRR signal and converts it into DC voltage. This DC voltage can be easily captured with an analog digital converter (ADC) or a digital multimeter.

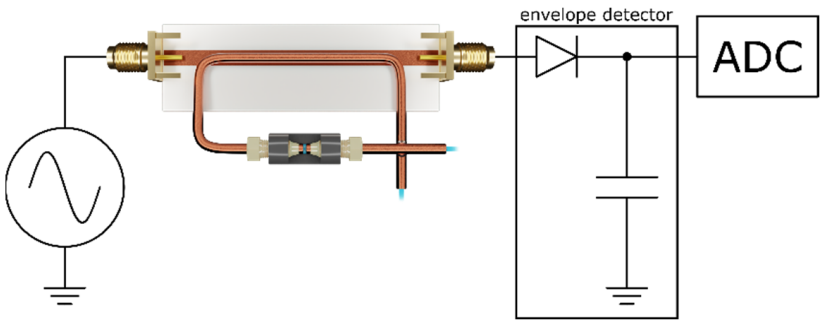

Figure 2. Basic concept of the new readout electronics consisting of a frequency-controlled sine-wave generator, the CaSRR, a demodulator (envelope detector), and an ADC.

At a constant frequency and constant split capacity, the voltage at the demodulation capacitor is constant. Changing the dielectric properties (permittivity, conductivity, and dielectric losses) of the split capacitor by an eluting peak from the LC column changes the frequency response leading to a different output voltage of the envelope detector. By measuring at a single frequency, a significant increase in the sampling rate of the new readout electronics is possible. This allows for significant averaging and reducing the noise level to reach a high signal-to-noise ratio (SNR).

The SNR of the system depends on the number of experimental variables such as the used excitation source, electromagnetic interference, temperature, frequency response of the CaSRR, and the ADC used. A higher bit count ADC in combination with a temperature compensated demodulator and excitation source can reduce the noise to a minimum.

The new readout electronics contains a controllable excitation source and two envelope detectors, one for the output of the excitation source and one for the transmitted output signal of CaSRR. A basic block diagram of the new readout electronics is shown in Figure 3.

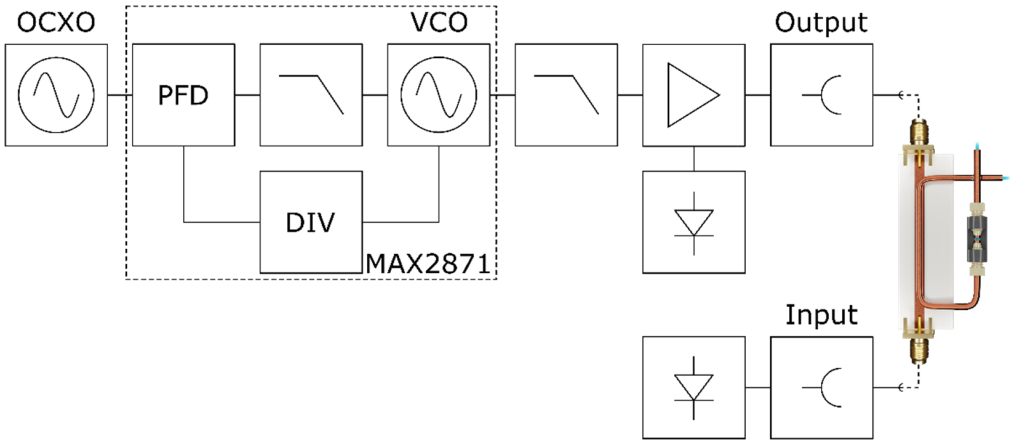

Figure 3. Block diagram of the developed new readout electronics, consisting of an oven-controlled oscillator (OCXO), the Analog Devices MAX2871 integrated PLL/VCO chip, an adjustable low-pass filter for filtering the harmonics, and an adjustable amplifier for the output. Both the output signal of the excitation source (CaSRR input) and the transmitted output signal of the CaSRR are recorded with demodulators.

The electronics is equipped with an oven-controlled crystal oscillator (OCXO) to reduce the frequency drift. As OCXO, an IQD IQOV-162-3 with a frequency tolerance of $\pm$500 ppb and a frequency stability of $\pm$20 ppb is used. This constant reference frequency is fed into an Analog Devices MAX2871 wide-frequency phase locked loop (PLL) with an integrated voltage-controlled oscillator (VCO). The MAX2871 compares the reference frequency against the divided output frequency with a phase frequency detector (PFD). The PFD generates a voltage that represents the phase difference of the two signals, and the voltage is then low pass filtered and controls the VCO in the MAX2871. Due to the divider between VCO and PFD, the output frequency can be set from 23.5 MHz to 6 GHz. Afterwards, this generated frequency is filtered with a low pass filter to reduce the harmonics for a clean output signal. Due to the wide frequency range of the system, multiple filters are used and automatically selected by the software controlling a RF switch (not shown). The different filters are needed to suppress the harmonics affecting the demodulated signal. In order to vary the output power and therefore the output voltage, a controllable attenuator and amplifier combination is implemented. Thus, it is possible to change the output frequency and the output power for different CaSRR setups. The integrated RF power detector chip Analog Devices HMC713LP3E converts the input RF power into DC voltage, as shown in Figure 4. The RF power is converted with $E_{Detector} = 17$ mV/dB in a range from 50 MHz to 2.7 GHz. For measuring the output power of the electronics and the transmitted power of the CaSRR, two identical demodulators are implemented. For fast and accurate data acquisition, a 16-bit (250 kS/s) ADC Linear Technology LTC1864 is used to capture the detector DC signals from the output power and the input power demodulator. The power detector is connected to the ADC via an operational amplifier Texas Instruments OPA2140 as a buffer. All additional resistors, inductors, and capacitors shown in Figure 4 are required to operate the power detector, ADC, and operational amplifier.

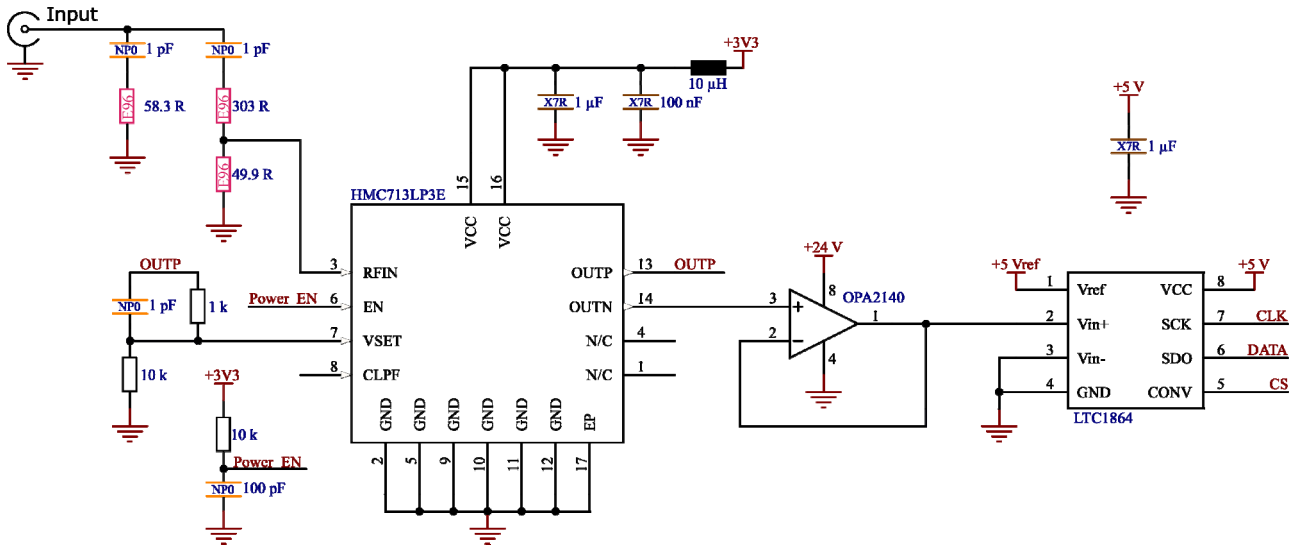

Figure 4. Circuit diagram of the input section including the power detector with the corresponding components and the ADC for analog-to-digital conversion.

To model the behavior of CaSRR, CST Studio Suite® was used, revealing the influence of the relative permittivity change on the frequency shift. Conductivity and dielectric losses are not considered in the following, as permittivity is expected to be the most important parameter when using sugars or 2-propanol in small concentrations in ultrapure water. However, dielectric losses and conductivity need to be considered when measuring other analytes that significantly change dielectric losses and conductivity of the eluate. In general, increasing the dielectric losses and conductivity damps the resonator, and thus broadens the resonance peak and shifts the resonance frequency both changing the demodulated output signal. Thus, SRR is sensitive to permittivity, dielectric losses, and conductivity, which can be an advantage when measuring such analytes. However, the eluent needs to have minimum dielectric losses and conductivity to minimize damping of the resonator, giving the highest sensitivity.

From the simulation, not shown here, a relationship between the relative permittivity change and the frequency shift is derived using a linear regression, as shown in Equation (1). From the derivative of the frequency response of the system, the maximum slope at the inflection points could be determined, resulting in E_{SRR} = 2.241 dB/MHz. From Equation (1), the sensitivity of the system can be determined to be $E = 0.15\Delta\varepsilon_r/\text{MHz}$, with $\Delta\varepsilon_r$ being the change in permittivity and Δf the frequency shift.

$$\Delta\varepsilon_r = -0.15 \cdot \frac{1}{\text{MHz}} \cdot \Delta f + 0.091 \tag{1}$$

Thus, $n_{averages}$ = 128 averages result in a minimum measurable frequency change Δf_{min} of 177 Hz calculated with Equations (2) and (3) with $V_{Ref} = 5$ V, $E_{Detector} = 17$ mV/dB the sensitivity of the HMC713LP3E RF detector, and $E_{SRR} = 2.241$ db/MHz the sensitivity of the simulated CaSRR. From this, a minimum measurable $\Delta\varepsilon_{r,min}$ change can be calculated with Equation (4).

$$\Delta f_{min} = \frac{V_{Ref}}{2^n} \cdot E_{Detector} \cdot \frac{1}{\sqrt{n_{averages}}} \cdot E_{SRR} \tag{2}$$

$$\Delta f_{min} = \frac{5\text{ V}}{2^{16}} \cdot \frac{\text{dB}}{17\text{ mV}} \cdot \frac{1}{\sqrt{128}} \cdot \frac{\text{MHz}}{2.241\text{ dB}} = 177\text{ Hz} \tag{3}$$

$$\Delta\varepsilon_{r,min} = 0.15 \cdot \frac{1}{\text{MHz}} \cdot 177\text{ Hz} = 26.55 \cdot 10^{-6} \tag{4}$$

This results in a theoretically measurable minimum permittivity change of $\Delta\varepsilon_{r,min} = 26.55 \cdot 10^{-6}$ calculated with Equation (4) and $\Delta f_{min} = 177$ Hz. A microcontroller operates the system and enables communication with a computer. With a self-developed National Instruments LabVIEW software, using either an operation at a constant excitation frequency or recording a frequency sweep, it is possible to determine the resonance frequency of the CaSRR. The constructed new readout electronics is shown in Figure 5 (top view of the final electronics on a four-layer Rogers 4350B PCB with dimension of 115 mm by 72 mm).

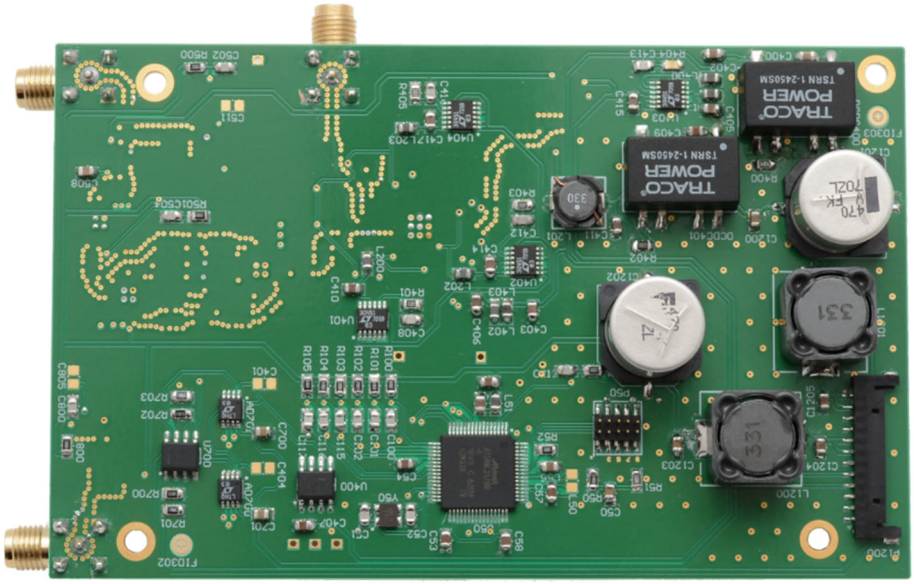

Figure 5. PCB of the new readout electronics (photo, top view) including all components required for power supply, control, and data acquisition.

The frequency stability and amplitude stability of the new readout electronics were measured with a Keysight Technologies N9030A PXA Signal Analyzer with the installed phase noise application Keysight Technologies N9068EMOD. The phase noise application had software version A.24.57 and allowed for fast and accurate measurement of the frequency stability and amplitude.

For measuring the frequency response of CaSRR, a vector network analyzer Rhode and Schwarz ZNL6 was used. The VNA and the matching cables Rhode and Schwarz ZV-Z192 were calibrated with a Rhode and Schwarz ZN-Z135 calibration kit.

To test the functionality of CaSRR with the developed new readout electronics, a Knaur HPLC system, as shown in Figure 6, with a built-in refractive index detector RID 2.1 L was coupled in series to CaSRR. HPLC consists of a solvent reservoir, a binary high-pressure pump P 6.1L with two 10 mL-heads, a degasser and a high-pressure mixing chamber, a 6-port-injectionvalve with 20 µL sample loop, a HPLC-column in a column thermostat CT 2.1, and a refractive index detector RID 2.1 L with a 15 µL flow cell volume. The refractive index detector has a maximum sample rate of 100 Hz with a noise of ±2.5 nRIU according to the datasheet.

First, the HPLC pump unit was used to determine the detection limit of CaSRR. The pump unit P 6.1L is capable of mixing and varying eluent mixtures with a very high degree of accuracy, and thus allows for automation of recording a calibration curve of different concentrations of 2-propanol and ultrapure water. The used mixtures were composed of 2-propanol (from 0% to 5% in 0.5% steps) in ultrapure water.

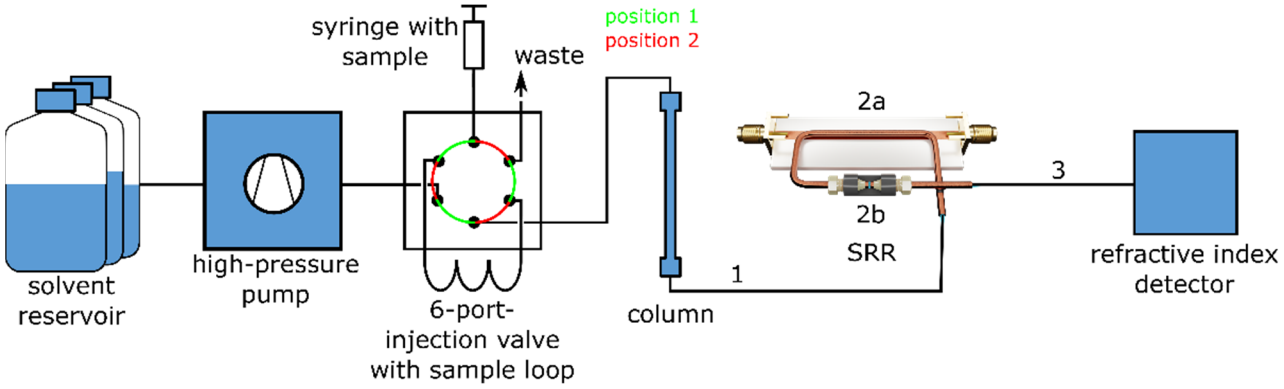

Figure 6. Schematic layout of the Knaur HPLC with the built-in SRR. The dead volumes between the HPLC column and the refractive index detector are as follows. (1) 30 cm capillary with inner diameter of 250 µm giving a dead volume of 14.7 µL, (2a) SRR capillary volume of 8.6 µL, (2b) split capacitor volume of 2.3 µL, and (3) 50 cm connecting capillary with inner diameter 250 µm giving a dead volume of 24.5 µL.

For the HPLC measurements, CaSRR was placed in series between the column and the refractive index detector. In this work, an YMC Europe YMC-Pack Polyamine II-column, a column specified for sugars and sugar alcohols after the HILIC-method, was used. The column had a length of 250 mm, a diameter of 4.6 mm, a particle size of 5 µm, and a pore size of 120 Å. The temperature of the column thermostat and the refractive index detector were set to 30 °C, the flow was 1 mL/min, and the sample volume was defined by the sample loop of 20 µL. The eluent was composed of 25% ultrapure water and 75% acetonitrile of HPLC-MS grade. The sample was a mixture of 125 mg/mL glucose and 115 mg/mL xylitol and, therefore was a mixture of sugar and sugar alcohol in ultrapure water.

The chemicals 2-propanol (Sigma product: 190764), acetonitrile (Sigma product: 1037252002), ultrapure water (Sigma product: 1037282002), D-(+)-glucose (Sigma product: G8270), and xylitol (Sigma product: 47844) that were used for all of the experiments were purchased from Sigma-Aldrich, Germany, with a purity of >99%.

For all of the measurements, the new readout electronics were housed in a thermally insulated box to minimize heat fluctuations and to ensure a constant temperature. This minimized the changes in the output signal, power detectors, and ADC.

3. Discussion

To demonstrate the capability of the new readout electronics, the frequency stability and amplitude stability were measured with the signal analyzer PXA N9030A. The results of the frequency and output power stability of the generated excitation output signal are shown in Figure 7. The average measured phase noise was 53.95 dBc/Hz at a bandwidth of 10 kHz. The settings for the frequency and amplitude stability measurements are shown in Table 1.

Table 1. N9030A measuring parameters.

Parameter	Value
Carrier frequency	1.0000005265 GHz
Average number	10
Sweep time for each measurement	17.81 ms
Measuring time	20 s
Resolution band width	10 kHz
Temperature	20 °C
Software version	A.24.57

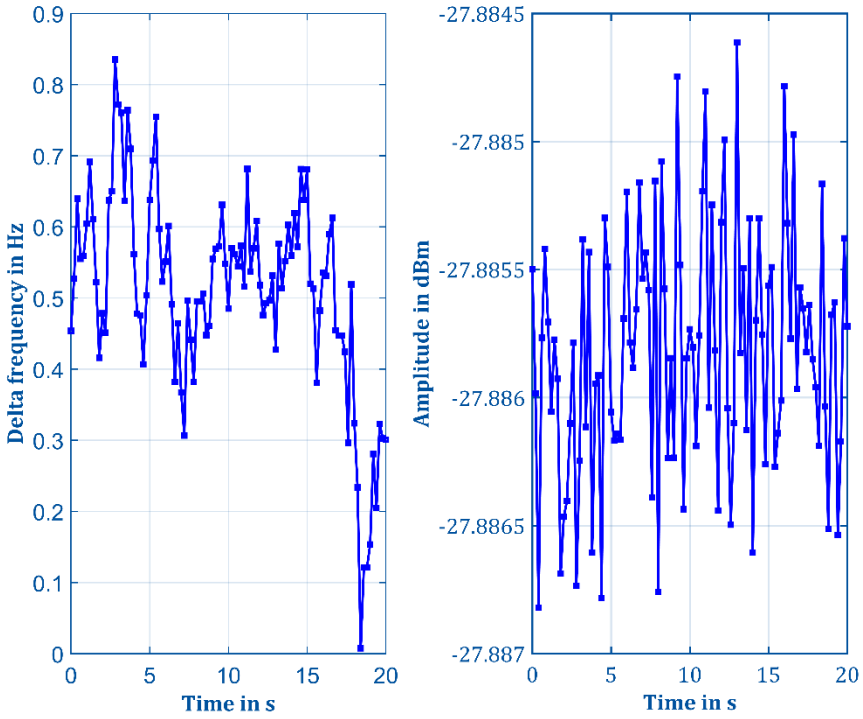

Figure 7. Output signal of new readout electronics measured at 1.0000005265 GHz over a time of 20 s. The left diagram shows the maximum frequency delta of 840 mHz and the right diagram shows that the amplitude is very stable with a maximum change from −27.8868 dBm to −27.8846 dBm.

The new readout electronics had very high frequency stability with a maximum frequency jitter of just 840 mHz within 20 s, which is the maximum possible measuring time of N9030A. In addition, the amplitude was very stable and changed only from −27.8868 dBm to −27.8846 dBm. The maximum sampling rate of either the output or transmitted power in combination with the LabVIEW software was at 5.4 kS/s. The sampling rate included averaging 128 measuring points by the microcontroller and the acquisition rate of the LabVIEW software with an average of 42 Hz. The sampling rate was of the same order of magnitude as the sampling rate of the refractive index detector.

Another optimization parameter was the excitation frequency for measuring the transmission response at a fixed frequency. Figure 8a shows the measured transmission response of the CaSRR loaded with 25% ultrapure water and 75% acetonitrile (used as eluent in the HPLC experiments) over a broad frequency range. The response of the split-ring resonator measured with the ZNL6 was low-pass filtered to achieve noise reduction for a better fit using MATLAB. The resonance frequency of the loaded CaSRR was 787.9 MHz. The black curve was fitted with a combination of five overlapping Gaussian peaks. The fit had an R^2 of 99.96%, leading to a good approximation of the measured CaSRR response.

To achieve the highest sensitivity of the system regarding the detection of resonance frequency shifts, the excitation frequency needed to be set to the frequency with the highest slope in the frequency response. We referred to this as the optimum excitation frequency. At this frequency, the amplitude change caused by a frequency shift was the highest and therefore best suited for measuring very small frequency shifts. For an ideal single Gaussian peak, the optimum excitation frequencies corresponded to the two symmetric inflection points. However, as the curve shown in Figure 8a is a superposition of five Gaussian peaks, the inflection points were at the plotted locations and so were the optimal measurement frequencies. Figure 8b shows the differentiation of the measured curve and the fitted curve from Figure 8a, to determine the optimum excitation frequencies with the highest slope.

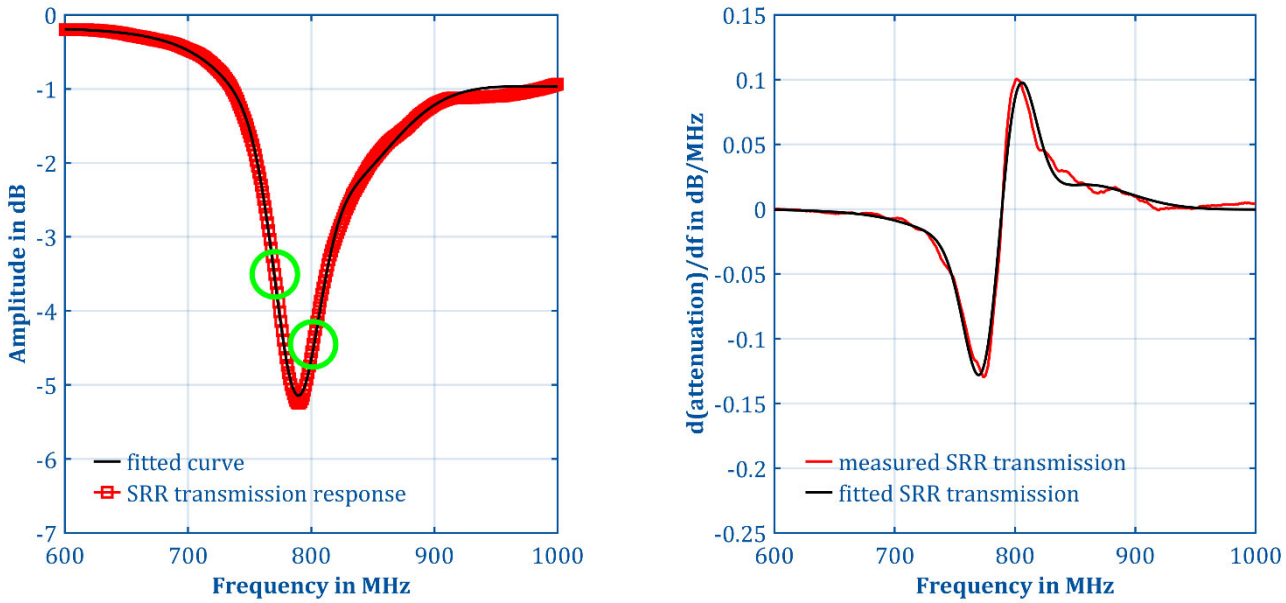

(**a**) (**b**)

Figure 8. (**a**) Measured (red squares) and fitted (black curve) transmission response of the CaSRR loaded with 25% ultrapure water and 75% acetonitrile used as an eluent in the HPLC experiments. The resonance frequency was 789.5 MHz, and the maximum attenuation was −5.246 dB. The green circles marked the optimum excitation frequencies below and above the resonance frequency for the highest sensitivity regarding the detection of resonance frequency shifts. (**b**) Differentiation of the measured and fitted CaSRR transmission response of the CaSRR loaded with eluent. The inflection points for the measured curve are at 774.5 MHz and at 801.5 MHz. For the fitted curve, the inflection point frequencies differ slightly, and are 770.264 MHz and 806.378 MHz, respectively.

The highest possible slope at the inflection points and therefore the highest possible sensitivity was at 774.5 MHz and at 801.5 MHz for the measured curve. For the fitted curve, the inflection point frequencies differed slightly and were 769.5 MHz and 805.5 MHz, respectively.

In order to investigate the optimum excitation frequency while considering the non-idealities of the electronics, the capillary split-ring resonator was simulated using MATLAB. Two additional factors had to be considered regarding the optimum excitation frequency, namely (a) the spectral impurity of the excitation frequency and (b) the expected extent of the frequency shift caused by a permittivity change. For modelling the spectral impurity of the excitation source, an ideal Gaussian peak was assumed with the previously measured phase noise of 53.95 dBc/Hz. The width of the Gaussian peak correlated to the measured phase noise of the excitation source from the new readout electronics. The measured jitter of the excitation frequency was small and was thus neglected here. For modelling CaSRR transmission, we used the fit of the frequency response from Figure 8a. To simulate a resonance frequency shift caused by a permittivity change, this fit was simply shifted accordingly. In the following, four resonance frequency shifts (each referred to the resonance frequency f_1 of CaSRR loaded with the eluent) were investigated, see Figure 9a. Each frequency response in Figure 9a was now multiplied with Gaussian peaks at different center frequencies representing the spectral impurity of the excitation source giving the frequency responses of the CaSRR when measured with the new readout electronics with imperfect excitation. The resulting shifted frequency responses were now subtracted from the non-shifted frequency response of the CaSRR loaded with the eluent, giving Figure 9b.

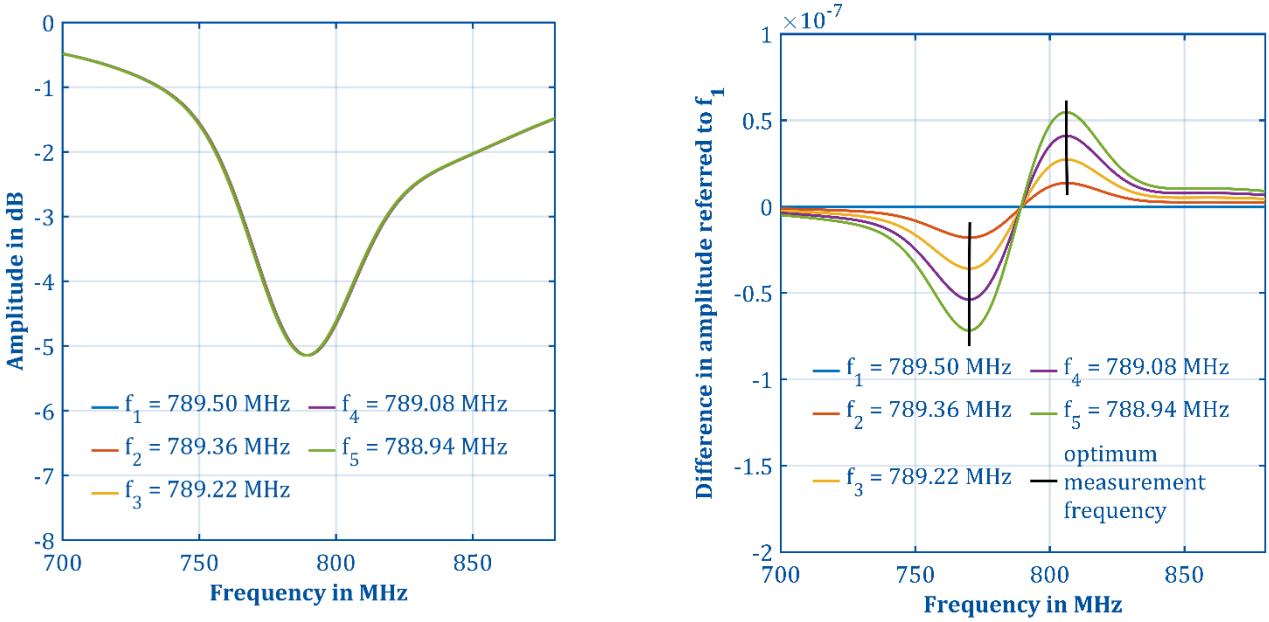

Figure 9. (**a**) Simulated frequency responses of CaSRR for different resonance frequencies (in 140 kHz steps). (**b**) Difference between the shifted frequency responses from the non-shifted frequency response, both including the impurity of the excitation source. The black lines mark the maximum differences in amplitude and thus the optimum excitation frequencies for the maximum sensitivity.

The highest sensitivity of CaSRR was always at the inflection points. For very large permittivity changes, it is advised to use an excitation frequency between the inflection points of the maximally shifted and non-shifted CaSRR response. However, the maximum permittivity change needs to be known in advance. Therefore, the optimum excitation frequency depends on the maximum permittivity shift expected in the application. For a shift of, e.g., $\Delta\varepsilon_r = 10{\cdot}10^{-3}$, which are 70 kHz, the optimum excitation frequency is at 770.232 MHz for the falling edge and at 806.346 MHz for the rising edge. The optimum excitation frequency is therefore about 32 kHz away from the inflection points and thus corresponds to Equation (5).

$$\mathrm{f_{optimum}} \approx \frac{\mathrm{f_{non-shifted}} - \mathrm{f_{shifted}}}{2} \tag{5}$$

As can be seen in Figure 10 that the CaSRR frequency response measured with our new readout electronics differed in frequency and amplitude from the measurement with the network analyzer shown in Figure 8a. This is due to the calibration just using through but not short, matching, and high impedance. However, in HPLC, this is not necessary, because we only measured the differences of the amplitude at the optimum excitation frequency. In HPLC, the shift in resonance frequency was so small, that the infliction points of the frequency response of the CaSRR loaded with the eluent were optimum. The inflection points are marked with green circles at 740 MHz and at 797 MHz. For 740 MHz, the sensitivity of CaSRR was at $E_{CaSRR,max} = \frac{1\ \mathrm{MHz}}{0.075\ \mathrm{dB}}$.

The sensitivity of CaSRR in combination with the new readout electronics was determined by measuring mixtures of ultrapure water and 2-propanol mixture. The HPLC pump unit was used to generate a step-wise increase and decrease of the 2-propanol concentration. As shown in Figure 11a, first an increasing concentration sequence of 1%, 2%, 3%, 4%, and 5% 2-propanol was measured, followed by a decreasing concentration sequence of 4.5%, 3.5%, 2.5%, 1.5%, and 0.5% 2-propanol in ultrapure water. This results in a stepwise change of the relative permittivity with the relative permittivity of ultrapure water being $\varepsilon_r = 29.3$

and 2-propanol being $\varepsilon_r = 18.6$ [25]. The relative permittivity of mixtures is calculated according to [25], with a minimum relative permittivity of $\varepsilon_r = 28.77$ for 5% 2-propanol.

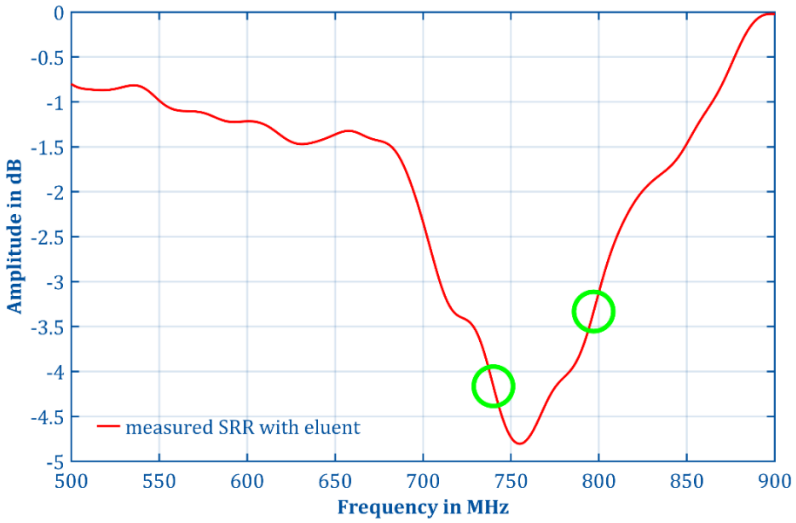

Figure 10. Measured transmission response (red) of the CaSRR loaded with the eluent and recorded with the new readout electronics. The resonance frequency was 755 MHz for the used eluent consisting of 25% ultrapure water and 75% acetonitrile, and the attenuation was −4.806 dB. The green circles mark the optimum excitation frequencies at 740 MHz and at 797 MHz for highest sensitivity regarding the detection of resonance frequency shifts.

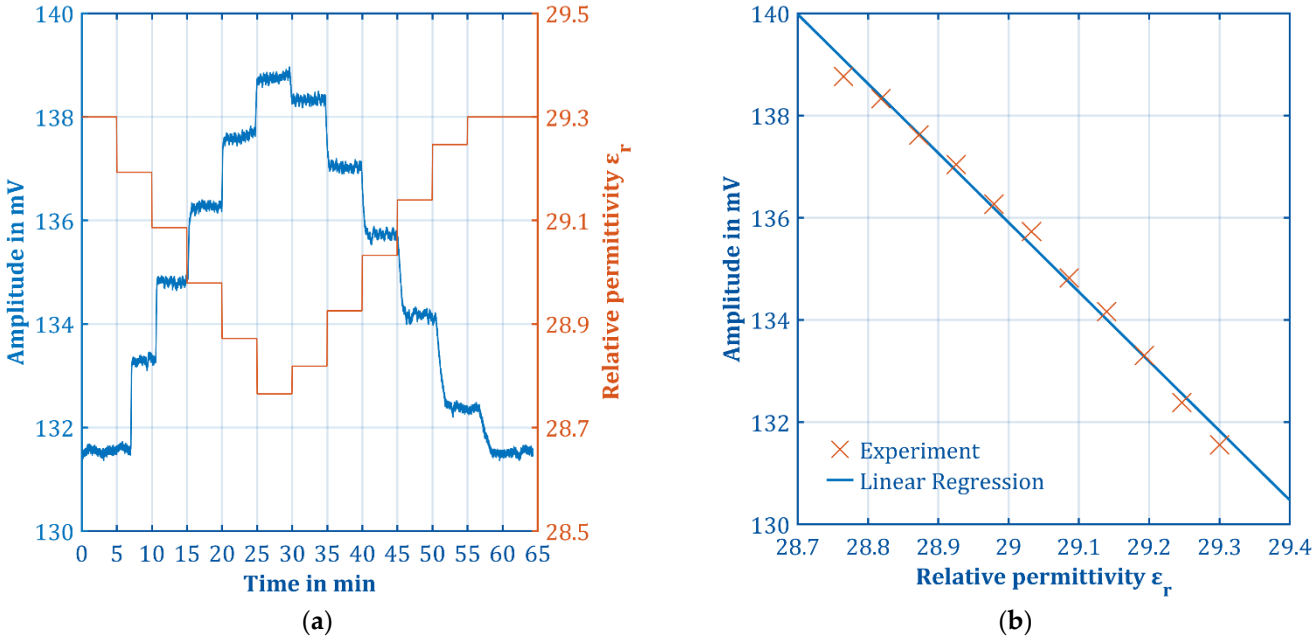

Figure 11. (**a**) Continuous measurement (capillary split ring resonator with new readout electronics) of 2-propanol (0% to 5%) in ultrapure water, giving relative permittivities from $\varepsilon_r = 29.3$ to $\varepsilon_r = 28.77$ (**b**) Mean value (orange cross) of the output signal of each relative permittivity step and linear regression (parameters given in Equation (6)) with an R^2 of 99.42%.

From the calibration curve shown in Figure 11a, the mean values of the output signal for each individual permittivity step (orange crosses) showed linear dependence of the output signal and relative permittivity, see Figure 11b. The linear regression is given in Equation (6). As the slope of the linear regression reflects the sensitivity $E = 13.586\text{mV}/\Delta\varepsilon_r$ of the measurement system, the measured noise of $U_{noise} = 0.051$ mV yields a detection

limit of $\Delta\varepsilon_{r,min} = 0.01126$ within an averaging time of only 24 ms. The detection limit refers to three times the standard deviation of the noise.

$$f(x) = -13.586\ \text{mV}\cdot\varepsilon_r + 529.9\ \text{mV} \quad (6)$$

By increasing the sample rate of the developed electronics to 120 kS/s, which is the maximum of ADC according to the datasheet of both the ADC and the microcontroller, the noise can be further decreased by averaging 2857 data points. This should allow for recording even the smallest changes of permittivity of $\Delta\varepsilon_r = 2.38{\cdot}10^{-3}$. Furthermore, a higher bit count ADC could be used to reduce the noise even further, and therefore increase the SNR of the measured signal.

To demonstrate the potential of the CaSRR with the new readout electronics, a HPLC chromatogram was recorded, see Figure 12. Therefore, the refractive index detector and the CaSRR were connected in series. The time delay between CaSRR and the refractive index detector is minimized using connecting capillaries with an inner diameter of only 250 µm, giving a dead volume of about 50 cm × 250 µm ≈ 24.5 µL. The time delay was determined to 1.5 s with a flow of $Q_{HPLC} = 1$ mL/min. The refractive index detector works in a differential-mode to eliminate changes in the eluent, so the first value was set to 0. This was also done for the first value of CaSRR. In the recorded spectrum of CaSRR, the peaks of water, glucose, and xylitol were directed to negative values due to the measuring frequency of 740 MHz at the inflection point with the highest sensitivity on the falling edge of the resonance peak. Water acted as an inert substance here, as it did not interact with the stationary phase of the column and was therefore not retarded. The dead time of the system determined from the retention time of water was 184 s. The retention time of xylitol was about 500 s, and the retention time of glucose was about 690 s.

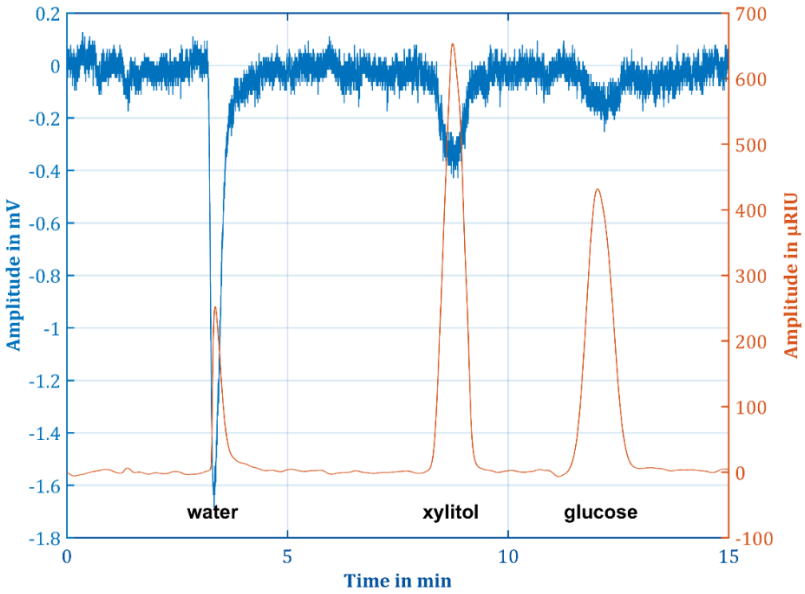

Figure 12. HPLC chromatogram of 125 mg/mL glucose and 115 mg/mL xylitol in ultrapure water, eluent 75% acetonitrile, 25% ultrapure water at 30 °C, measured with CaSRR (blue) at 740 MHz (inflection point) and refractive index detector (orange).

It needs to be noted that the concentrations of 125 mg/mL glucose and 115 mg/mL xylitol were diluted by HPLC. The dilution factor DF can be calculated from the peak width at half maximum w_{hm}, the flow rate Q_{HPLC}, and the volume of the sample loop $V_{sample-loop}$, according to Equation (7).

$$DF = \frac{V_{sample-loop}}{w_{hm}\cdot Q_{HPLC}} = \frac{20\ \mu\text{L}}{1\text{min}\cdot 1\ \text{mL/min}} = 0.02 \quad (7)$$

For a peak width at a half maximum of about $w_{hm} = 1$ min, a sample loop with $V_{sample-loop} = 20$ µL and $Q_{HPLC} = 1$ mL/min, the concentration at the detector was 2.5 mg/mL for glucose and 2.3 mg/mL for xylitol (dilution factor of DF = 0.02). In Figure 12, CaSRR is compared to the refractive index detector, which has a significantly higher sensitivity to sugars and sugar-derivatives. As permittivity and refractive index are related according to Equation (8), this can be explained by the different measuring frequencies [26] (pp. 232–235).

$$n(f) = \sqrt{\varepsilon_r(f)} \tag{8}$$

Obviously, at 740 MHz (CaSRR) the permittivity change caused by sugars and sugar-derivatives dissolved in ultrapure water is less pronounced compared to the light (450 nm to 490 nm and 630 nm to 700 nm) (refractive index detector). This high difference in frequency has different effects on the polarization properties at 740 MHz mainly orientational polarization effects occur and at light frequencies of 428 THz to 666 THz, atomic polarization effects occur [26] (pp. 232–235). While there is room for vast improvements in the signal to noise ratio, this first chromatogram demonstrates the basic feasibility of CaSRR and the new readout electronics for application in HPLC.

4. Conclusions

In this work, we demonstrated a new capillary split-ring resonator (CaSRR) with a fast but simple new readout electronics for application in HPLC. For easy integration with HPLC, the split-ring was formed by capillaries. Changes in the electromagnetic properties of the eluent implied by the analytes passing the split capacitor of the split-ring resonator were detected by a shift in resonance frequency. For fast readout, the resonance frequency was not recorded. Instead, by demodulating a constant excitation frequency within the frequency response of CaSRR, the amplitude of the demodulated signal correlated to the shift in resonance frequency. If, e.g., the permittivity at the split capacitor changed, a shift in the filter response and thus a change in the demodulated signal results. The amplitude of the demodulated signal corresponded to permittivity change. This approach is well suited for the rapid detection of even the smallest permittivity changes of $\Delta\varepsilon_r = 11.26 \cdot 10^{-3}$, as it offers a significantly larger number of averages per measuring time (within 24 ms up to 5.4 kS/s) and thus a significantly better signal-to-noise ratio compared to any frequency sweeping method to record the resonance frequency. As only one frequency was used, the choice of this measuring frequency was crucial in terms of sensitivity. In the current setup, the optimum excitation frequency was at the inflection points of the filter response. For proof-of-principle, a chromatogram of glucose and xylitol dissolved in water was recorded.

Author Contributions: Conceptualization, M.H., K.J.D. and A.V.G.; methodology, M.H. and K.J.D.; software, M.H., K.J.D. and A.V.G.; validation, M.H. and K.J.D.; formal analysis, M.H.; investigation, M.H. and K.J.D.; data curation, M.H.; writing—original draft preparation, M.H.; writing—review and editing, K.J.D., A.V.G. and E.-F.S.; visualization, M.H.; supervision, S.Z.; project administration, S.Z.; funding acquisition, S.Z. All authors have read and agreed to the published version of the manuscript.

Funding: This research received no external funding.

Data Availability Statement: The data are available upon request.

Acknowledgments: We thank Nic Solle and Christian Beckemeier for their help during this work. We want to acknowledge Martin Lippmann and Cameron Naylor for their advice during editing.

Conflicts of Interest: The authors declare no conflict of interest.

References

1. Torun, H.; Cagri Top, F.; Dundar, G.; Yalcinkaya, A.D. An antenna-coupled split-ring resonator for biosensing. *J. Appl. Phys.* **2014**, *116*, 124701. [CrossRef]
2. Verma, A.; Bhushan, S.; Tripathi, P.N.; Goswami, M.; Singh, B.R. A defected ground split ring resonator for an ultra-fast, selective sensing of glucose content in blood plasma. *J. Electromagn. Waves Appl.* **2017**, *31*, 1049–1061. [CrossRef]

3. Reinecke, T.; Walter, J.-G.; Kobelt, T.; Ahrens, A.; Scheper, T.; Zimmermann, S. Design and evaluation of split-ring resonators for aptamer-based biosensors. *J. Sens. Sens. Syst.* **2018**, *7*, 101–111. [CrossRef]
4. Reyes-Vera, E.; Acevedo-Osorio, G.; Arias-Correa, M.; Senior, D.E. A Submersible Printed Sensor Based on a Monopole-Coupled Split Ring Resonator for Permittivity Characterization. *Sensors* **2019**, *19*, 1936. [CrossRef] [PubMed]
5. Galindo-Romera, G.; Javier Herraiz-Martinez, F.; Gil, M.; Martinez-Martinez, J.J.; Segovia-Vargas, D. Submersible Printed Split-Ring Resonator-Based Sensor for Thin-Film Detection and Permittivity Characterization. *IEEE Sens. J.* **2016**, *16*, 3587–3596. [CrossRef]
6. Meyne, N.; Cammin, C.; Jacob, A.F. Accuracy enhancement of a split-ring resonator liquid sensor using dielectric resonator coupling. In Proceedings of the 20th International Conference on Microwave, Radar and Wireless Communicatons (MIKON), Gdansk, Poland, 16–18 June 2014; pp. 255–258.
7. Chretiennot, T.; Dubuc, D.; Grenier, K. A Microwave and Microfluidic Planar Resonator for Efficient and Accurate Complex Permittivity Characterization of Aqueous Solutions. *IEEE Trans. Microw. Theory Techn.* **2013**, *61*, 972–978. [CrossRef]
8. Rowe, D.J.; al-Malki, S.; Abduljabar, A.A.; Porch, A.; Barrow, D.A.; Allender, C.J. Improved Split-Ring Resonator for Microfluidic Sensing. *IEEE Trans. Microw. Theory Techn.* **2014**, *62*, 689–699. [CrossRef]
9. Zebiri, C.; Mshwat, W.; Kosha, J.; Lashab, M.; Elfergani, I.; Sayad, D.; Mosbah, S.; Rodreguez, J.; AlYasir, Y.; Abd-Alhameed, R. A Metamaterial-Based Microwave Sensor for Liquid Dielectrics Characterization. In Proceedings of the 1st International Multi-Disciplinary Conference Theme: Sustainable Development and Smart Planning, IMDC-SDSP 2020, Cyberspace, 28–30 June 2020.
10. Shakoor, O.; Taylor, R.B.; Behrens, R.H. Assessment of the incidence of substandard drugs in developing countries. *Trop. Med. Int. Health* **1997**, *2*, 839–845. [CrossRef] [PubMed]
11. Di Stefano, V.; Avellone, G.; Bongiorno, D.; Cunsolo, V.; Muccilli, V.; Sforza, S.; Dossena, A.; Drahos, L.; Vékey, K. Applications of liquid chromatography-mass spectrometry for food analysis. *J. Chromatogr. A* **2012**, *1259*, 74–85. [CrossRef] [PubMed]
12. Buttler, T.A.; Johansson, K.A.J.; Lo Gorton, G.O.; Marko-Varga, G.A. On-line fermentation process monitoring of carbohydrates and ethanol using tangential-flow filtration and column liquid chromatography. *Anal. Chem.* **1993**, *65*, 2628–2636. [CrossRef]
13. Swartz, M. HPLC Detectors: A Brief Review. *J. Liq. Chromatogr. Relat. Technol.* **2010**, *33*, 1130–1150. [CrossRef]
14. Lakowicz, J.R. *Principles of Fluorescence Spectroscopy*; Springer: Boston, MA, USA, 2006; ISBN 978-0-387-31278-1.
15. Wahab, M.F.; Dasgupta, P.K.; Kadjo, A.F.; Armstrong, D.W. Sampling frequency, response times and embedded signal filtration in fast, high efficiency liquid chromatography: A tutorial. *Anal. Chim. Acta* **2016**, *907*, 31–44. [CrossRef] [PubMed]
16. Dehning, K.J.; Hitzemann, M.; Fisahn, S.; Zimmermann, S. Split-ring resonator: A new detector in liquid chromatography. *Dresdner Sens.-Symp.* **2019**, *14*, 167–171. [CrossRef]
17. Gehl, A.; Zimmermann, S. Ein neues Detektorkonzept für die Flüssigchromatographie basierend auf einem Split-Ring-Resonator / A new detector concept for liquid chromatography based on a split-ring resonator. *tm-Tech. Mess.* **2018**, *85*, s33–s37. [CrossRef]
18. Dehning, K.J.; Hitzemann, M.; Sterr, E.-F.; Zimmermann, S. P8.9—Split-Ring Resonator as Detector for Liquid Chromatography. *Dresdner Sens.-Symp.* **2021**, *15*, 285–289. [CrossRef]
19. Sayed, M.; Ferrero, A.; Teppati, V. *Modern RF and Microwave Measurement Techniques*; Cambridge University Press: Cambridge, UK, 2013; ISBN 9781139567626.
20. Chuma, E.L.; Iano, Y.; Fontgalland, G.; Bravo Roger, L.L. Microwave Sensor for Liquid Dielectric Characterization Based on Metamaterial Complementary Split Ring Resonator. *IEEE Sens. J.* **2018**, *18*, 9978–9983. [CrossRef]
21. Tumurbaatar, B.; Kim, M.-J.; Park, C.-H.; Kim, C.S. A portable and computer-simulation analysis for the real-time measurement of the QCMD systems for the biomedical application. *Sens. Bio-Sens. Res.* **2018**, *21*, 75–81. [CrossRef]
22. Omar, A.S.; Maslenikov, A.B.; Belenky, V.G.; Ogourtsov, S.G.; Yu, K.B. Accurate microwave resonant method for complex permittivity measurements of liquids [biological]. *IEEE Trans. Microw. Theory Techn.* **2000**, *48*, 2159–2164. [CrossRef]
23. Lee, H.-J.; Yook, J.-G. Biosensing using split-ring resonators at microwave regime. *Appl. Phys. Lett.* **2008**, *92*, 254103. [CrossRef]
24. Baena, J.D.; Bonache, J.; Martin, F.; Sillero, R.M.; Falcone, F.; Lopetegi, T.; Laso, M.; Garcia-Garcia, J.; Gil, I.; Portillo, M.F.; et al. Equivalent-circuit models for split-ring resonators and complementary split-ring resonators coupled to planar transmission lines. *IEEE Trans. Microw. Theory Techn.* **2005**, *53*, 1451–1461. [CrossRef]
25. Endress+Hauser GmbH+Co. KG. *Dielectric Constant (DC Value) Compendium*; Endress+Hauser GmbH+Co. KG: Maulburg, Germany, 2014.
26. Andreas Küchler. *Hochspannungstechnik*; Springer: Berlin/Heidelberg, Germany, 1996; ISBN 978-3-662-22000-9.